ORIGINAL RESEARCH

Sensitivity of friction coefficients, material constitutive laws and yield functions on the accuracy of springback prediction for an automotive part

Slim Ben-Elechi[1] · Mourad Khelifa[2] · Riadh Bahloul[1]

Abstract

High Strength Steel is more used in automotive industry to combine safety improvements and weight reductions of the vehicles. However, these steels raise new challenges for manufacturer, especially for springback and its prediction. Finite Element Analysis is widely used for the prediction of springback but accuracy is strongly depending on numerical as well as physical parameters. Such parameters affecting prediction are for example frictional behavior, constitutive model, loci function. In this paper the sensitivity of friction coefficients and the influence of some material laws on the springback prediction were studied and analyzed in details. Several numerical models are investigated in this work in order to allow the different aspects of materials mechanical behavior to be better described: isotropic work-hardening (Swift, Hockett-Sherby, SHS), isotropic-kinematic hardening, yield loci (Hill 48, Hill 90 and Barlat 91). In this study, we use an industrial example of the deep drawing process: the side sill closing with the material steel TRIP800. All the simulations are carried out with the commercial code Pam-Stamp 2G and comparison with the experimental results are presented.

Keywords Springback · Measurements · F. E simulation · Work-hardening · Materials models · Yield loci

Introduction

High Strength Steel (HSS) and Very High Strength Steel (VHSS) are more used in automotive industry to reduce the weight and to improve the safety of the vehicles. However, several undesirable phenomena are observed after the forming of such materials. Springback is one of the critical problems that appear when high strength steel is used. Many researchers have investigated the springback phenomenon using experience and finite element analysis (FEA). FEA is widely accepted for the prediction of formability issues such as thinning, wrinkles, and fracture but the FEA has not achieved the same level of accuracy in springback prediction. This is a complicated task because accuracy is strongly depending on numerical as well as physical parameters.

The frictional is a parameter that has a big impact on springback prediction, but it has been often simplified for the industrial forming by adopting the classical Coulomb's law. The frictional behaviour is influenced by many factors such as lubricant, material properties and process conditions. Several researchers have shown that the friction coefficient is not constant during forming process and it varies depending on loading conditions, temperature, and sliding velocity. Grueebler and Hora [1] investigated temperature and velocity dependence of the friction for a biaxial stretching test, the numerical results showed a good correlation with measurements. Santos and Teixeira [2] studied the U-bending process and proposed different values of the friction coefficient on different contact regions. Keum et al. [3] studied the forming of aluminium alloy and steel. They expressed the friction coefficient as a function of sheet properties, lubricant viscosity,

✉ Slim Ben-Elechi
slim.benelechi@issig.u-gabes.tn

Mourad Khelifa
mourad.khelifa@univ-lorraine.fr

Riadh Bahloul
bahloul_riadh@yahoo.fr

1 Laboratory of Mechanical Engineering, National Engineering School of Monastir, University of Monastir, Avenue Ibn Eljazzar, 5019 Monastir, Tunisia

2 University of Lorraine, LERMAB, EA 4370, 27 rue Philippe Séguin, 88051 Epinal, France

tool geometry and forming speed. Kim et al. [4] proposed more realistic characterisation of friction behaviour of HSS considered an experimental system based on contact pressure. This kind of approach requires a testing device that is very expensive. The friction behavior has been simplified in most industrial applications, i.e., the coefficient of friction has usually been supposed to be constant.

In the last decade, the numerical development for springback analysis has been mainly relying on material mechanical behavior and Finite element technique. Julsri et al. [5] studied the springback of two grades of steel using macroscale and microscale representative volume elements. Lin et al. [6] studied the effect of constitutive model on the springback prediction of of two materials: advanced high strength steel MP980 and aluminum alloy 6022-T4. Their numerical results are compared to measurements of stamped U-channel. Ben-Elechi et al. [7] developed a fast-deep drawing and springback of sheet metals using an improved inverse approach method. The obtained results showed a good accuracy of springback predictions. Quadfasel et al. [8] analyzed the springback of three high manganese TWIP-steels using U-bending test. The bending angle of U-profiles obtained after springback showed a higher springback prediction than expected. Lee et al. [9] implemented a new friction model based on the macroscopically observation of frictional behavior. The influences of the material and friction models for the springback prediction in U-draw/bending were presented. Zhang et al. [10] studied springback prediction of U bending based on analytical model and Hill's1948 yield criteria. Laurent et al. [11] proposed experimental and numerical studies of springback for the split-ring test. The obtained results showed that the yield criteria presented higher impact on simulation accuracy than the hardening law. In the same context, Oliveira et al. [12] simulated the springback of draw-bending for DC06/DP600 and evaluated several hardening models. Broggiato et al. [13] studied the Chaboche nonlinear kinematic hardening model within the FEM code. In their work, experimental and FEA results are compared. Sumikawa et al. [14] analyzed the springback of curved hate shape part using two high strength steel. The influence of Young's modulus, Bauschinger effect, elastic and plastic anisotropy on springback predictions was presented. Komgrit et al. [15] proposed a new technique to reduce the U bending springback of High-Strength Steel (HSS) by both numerical and experimental investigations. In their original forming method, a kinematic hardening and the Yoshida–Uemori model was used.

In conclusion of this part of literature review, the friction and material mechanical behavior are parameters that have big impact on springback prediction. Moreover, there has been no study in which friction and material behavior parameters, that is, isotropic work-hardening isotropic-kinematic hardening and yield loci were considered simultaneously in springback analysis of industrial application.

The aim of this work is to investigate springback effects of an automotive part by both experiments and FE simulations. The forming of side sill closing of a car was studied in order to analyze the sensitivity of friction coefficients, the material constitutive laws and the yield functions on the accuracy of springback prediction. All numerical simulations are carried out with the commercial code Pam-Stamp 2G.

Constitutive models

During the forming process the elastoplastic modeling is adopted and the material is initially stress-free. The plastic part ε^p follows a flow rule and is derived from the yield function. The model is based on Hills 1948 yield criterion and the relationship defining the equivalent stress σ is given by the Eq. (1):

$$\overline{\sigma}^2 = \left(\sigma' - X\right) : M : \left(\sigma' - X\right) \tag{1}$$

Where M is a symmetric tensor, which is function of the anisotropy parameters of the Hill'48 quadratic yield function. σ' represents the Cauchy's deviatoric stress tensor and X represents the back-stress tensor.

The evolution of the flow stress with plastic work is:

$$\sigma = f\left(\overline{\varepsilon}^p\right) \tag{2}$$

In this study three laws (Swift, Hockett-Sherby and SHS) are implemented to describe the isotropic work-hardening and another one, a combined isotropic-kinematic hardening law (Mixed) to provide a flexible model, simultaneously describing the change in size and position of the center of the yield surface.

- Swift law:

$$\sigma = K\left(\varepsilon_0 + \overline{\varepsilon}^p\right)^n \tag{3}$$

- Hockett-Sherby law:

$$\sigma = \sigma_{sat} - (\sigma_{sat} - \sigma_0)\exp\left(-n \ \overline{\varepsilon}^p\right) \tag{4}$$

- SHS law:

$$\sigma = (1-\alpha)K\left(\varepsilon_0 + \overline{\varepsilon}^p\right) + \alpha\left\{\sigma_{sat} - (\sigma_{sat} - \sigma_0)\exp\left(-n\ \overline{\varepsilon}^p\right)\right\} \quad (5)$$

where $K, \varepsilon_0, n, \sigma_{sat}, \sigma_0, \alpha$ are the constitutive models parameters for the swift, Hockett-Sherby and SHS law.

- Mixed law:

The Mixed law describes isotropic and kinematic hardening and can be expressed using two internal states variables. The first variable is a scalar: R, describing the isotropic hardening and the second variable is a tonsorial X, describing the kinematic hardening. X can be described by the following equation:

$$\dot{X} = C_X\left[\frac{X_{sat}}{\overline{\sigma}}\left(\sigma' - X\right) - X\right]\dot{\overline{\varepsilon}}^p \quad (6)$$

where C_X represents the saturation rate of X and X_{sat} is a material parameter representing the saturation value of the norm $|X|$ of the back stress, Lemaitre and chaboche [16].

The isotropic hardening evolution gives the variation of the yield surface size Y, expressed by

$$Y = Y_0 + R \quad (7)$$

Y_0 is the initial value of the yield stress and R is the saturation of flow stress given by the following equation:

$$R = R_{sta}\left(1 - \exp\left(-C_r\overline{\varepsilon}^P\right)\right) \quad (8)$$

where C_r represents the saturation rate of R and R_{sat} describes its saturation value.

Yield functions

The yield criteria describe the material transition from the elastic to plastic behavior. In this paper three yield functions are studied: Hill 48, Hill 90 and Barlat 91.

Hill 48 yield criterion [20] is one of the simplest and most used yield functions which it can be easily implemented in FE codes for the simulation of forming processes. The quadratic yield criterion is given as follow:

$$2f\left(\sigma_{ij}\right) = F\left(\sigma_{yy} - \sigma_{zz}\right)^2 + G(\sigma_{zz} - \sigma_{xx})^2 + H\left(\sigma_{xx} - \sigma_{yy}\right)^2 \quad (9)$$

$$+ 2\left(L\sigma_{yz}^2 + M\sigma_{zx}^2 + N\sigma_{xy}^2\right) = 1$$

where F, G, H, L, M and N are the material constants and x, y and z are the orthogonal axes of orthotropic.

According to Hill's plasticity conditions (Dasappa et al., [17]), and in case of plane stress problem($\sigma_{zz} = \sigma_{yz} = \sigma_{zx} = 0$), Hill 48 quadratic yield function will be reduced to:

$$2f\left(\sigma_{ij}\right) = (G+H)\sigma_{xx}^2 + (F+H)\sigma_{yy}^2 - 2H\sigma_{xx}\sigma_{yy} + 2N\sigma_{xy}^2 = 1 \quad (10)$$

where $\sigma_{xx}, \sigma_{yy}, \sigma_{zz}, \sigma_{yz}, \sigma_{zx}$ and σ_{xy} are the components of the Cauchy stress tensor defined in the orthotropic frame, σ_{ij} is the equivalent tensile stress. $\sigma_{xx}, \sigma_{yy}, \sigma_{zz}$ are defined by stresses in the rolling direction (x), transverse direction (y), and thickness direction (z), respectively; while σ_{xy}, σ_{yz}, and σ_{zz} are the shear stresses in xy, yz, and zx directions.

The material parameters F, G, H, and N can be described using normal anisotropy in $0°, 45°$ and $90°$ directions.

$$F = \frac{r_0}{r_{90}(r_0 + 1)}, G = \frac{1}{r_0 + 1}, G = \frac{1}{r_0 + 1}, H = \frac{r_0}{r_0 + 1}, N$$

$$= \frac{(r_0 + r_{90})(1 + 2r_{45})}{2r_{90}(r_0 + 1)} \quad (11)$$

The yield criteria proposed by Hill in 1990 (Hill 90) is based on a non-quadratic yield function as opposed to the Hill 48 quadratic yield function. Hill 90 function seems to be well adapted because it is able to take into account different behaviors during the bending/unbending phase. The Hill 90 criterion model is more convex than the Hill 48 model, but the computing time during numerical simulations is increased [18].

The parameters of Hill 90 yield function are determined from the uniaxial tension tests along three directions i.e., 0°, 45° and 90° and from bi-axial tension or shear test. The yield criterion is formulated by:

$$\left|\sigma_{xx} + \sigma_{yy}\right|^m + \alpha^m\left[\left(\sigma_{xx} - \sigma_{yy}\right)^2 + 4\sigma_{xy}^2\right]^{\frac{m}{2}}$$

$$+ \left[\sigma_{xx}^2 + \sigma_{yy}^2 + 2\sigma_{xy}^2\right]^{\frac{m}{2}-1}\left\{\beta\left(\sigma_{xx}^2 - \sigma_{yy}^2\right) + \gamma\left(\sigma_{xx} - \sigma_{yy}\right)^2\right\}$$

$$= (1 + \alpha^m + \beta + \gamma)\left(\sigma_{yy}^1\right)^m = \left(2\sigma_{yy}^b\right)^m \quad (12)$$

where α, β, γ, m are constant parameters of material, σ_{yy}^1 and σ_{yy}^b represent the yield stress under uni-axial tension and equi-biaxial tension, respectively.

The third yield function considered in this study is related to Barlat 91 criterion which will makes it possible to represent more general the plasticity convexity than HILL 48 and HILL 90 criterions. Its formulation can be described as follows [18]:

$$g = |S_1 - S_2|^m + |S_2 - S_3|^m + |S_3 - S_1|^m = 2Y^m \quad (13)$$

where S_1, S_2 and S_3 are the principal values of the isotropic plastic equivalent deviatory stress tensor **S**. The exponent m represents the shape of the yield surface that depends on the structure of the material. These previous values are determined from the following matrix:

$$\begin{bmatrix} [(b+c)\sigma_{11}-c\sigma_{22}-b\sigma_{33}]/3 & h\sigma_{12} & g\sigma_{13} \\ h\sigma_{12} & [(a+c)\sigma_{22}-c\sigma_{11}-a\sigma_{33}]/3 & f\sigma_{23} \\ g\sigma_{13} & f\sigma_{23} & [(a+b)\sigma_{33}-b\sigma_{11}-a\sigma_{22}]/3 \end{bmatrix} \tag{14}$$

The different coefficients a, b, c, f, g, h are obtained from uniaxial and shear yield stresses in the directions of the symmetry axes using a Newton-Raphson numerical procedure. The exponent m represents the severity of the texture and can take any real value larger than 6 (Barlat et al., [19]).

Application

In the current study an industrial application was treated experimentally and numerically using an advanced high strength steel sheet (TRIP800). The effects of friction coefficient and material proprieties on the accuracy of the springback are investigated. Figure 1 shows the position of the real part of side sill closing in the automotive structure.

The experimental system used for this project is depicted in Fig. 2. It is composed of Deep drawing hydraulic press and data acquisition systems maintained by a digital interface board utilizing a specialized computer program.

The simulation of the deep drawing process is conducted in two steps: the forming and the springback analysis. The forming simulation is done by explicit time integration and the springback is done by the implicit time integration. The tools (punch, die and blank holder) were modeled as rigid bodies, and the blank was described using shell elements with five integration points in the thickness. Throughout this work, the average element size of the uniform mesh was about 8 mm in width and in length. The refinement level of the elements was set to 4 so that the smallest elements had a size of 2 mm. The tool setup imported in the numerical simulation software

is shown in Fig. 3. The numerical tests were performed with a blank holder force of 38 tones.

The initial sheet thickness of the side sill closing is 1.2 mm. All simulations are carried out using Pam-Stamp 2G software with a fixed set of numerical parameters in order to numerically evaluate the influence of the material models on the prediction of springback. Figure 3 presents three-dimensional exploded view of the initial configuration of tools used for the simulation of the deep drawing process.

Results

In order to have an idea about the sensitivity of springback prediction to the material parameters, first we will present the sensitivity of the springback to the friction coefficients (considered as reference). Then, we will investigate the obtained results for the different material parameters: constitutive laws (isotropic hardening and kinematic-isotropic hardening) and yield functions (Hill 48, Hill 90 and Barlat 91). All numerical results will be compared with measurements.

Effects of friction coefficient

The friction is used as a reference parameter to compare the influence of the different material models. It was recognized that the contact behavior governed by the coefficient of friction is an important parameter in deep drawing process that has a critical influence on the springback prediction, for this reason we start our study with this parameter. Three friction coefficients (μ=0.08, μ=0.12 and μ=0.16) are chosen to evaluate the influence of this parameter on the springback prediction. The material TRIP800 was used and the SHS law was implemented on Pam-Stamp 2G software. The results obtained after forming given in terms of springback for the different coefficients of friction are presented below. Figure 4a shows the displacement iso-values obtained after springback in case of coefficient of friction μ=0.12. The distance is oriented within the normal. This last is also oriented in the interior of the side sill closing, so the positive values represent a displacement to the inside and the negative values represent a

Fig. 1 Real part of side sill closing

Fig. 2 Experimental trials of deep drawing: **a)** Deep drawing hydraulic press and data acquisition systems **b)** Zoom of the tooling setup
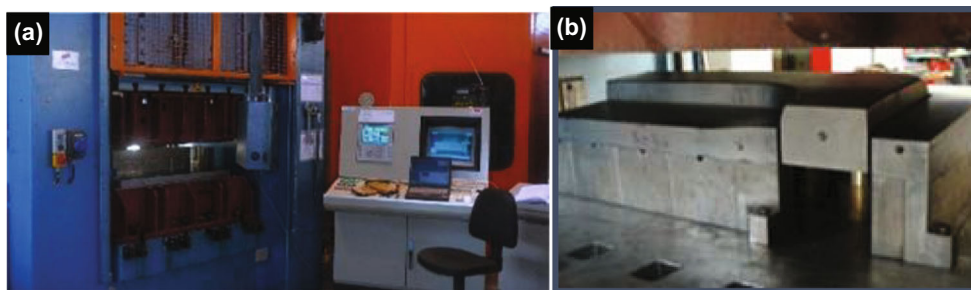
displacement to the outside. Two phenomena are produced during the springback: the cambering at the middle of the side sill closing and the twist at the bottom part. The maximum and minimum displacement obtained after springback appearance are 22.3 mm and −14 mm, respectively. In the same manner, the relative displacement resulting from springback prediction with a value of friction coefficient μ=0.16 is illustrated in Fig. 4b. From this contour plot, the maximum displacement obtained after springback is 24.9 mm and the minimum value is −14.4 mm. Figure 4c depicts the relative displacement between the two results corresponding to the friction coefficients of μ= 0.12 and μ= 0.16. As it can be noted from this figure, the maximum variation between the two results is ΔU_{max} = 2.56 mm and the minimum one is ΔU_{min} = −2.44 mm. In order to better understand the evolution of springback we chose the relative variation between the two results expressed in percentage form. It was calculated by the following formulation:

$$\%Variation = \frac{Variation\ between\ the\ two\ results\ (Fig.\ 4c)}{Variation\ of\ the\ reference\ result\ (Fig.\ 4a)} \times 100 \quad (15)$$

The calculated percentage of the relative variation of the displacement compared to these two coefficients of friction (μ=0.12 and μ=0.16) could be summarized as follow: $\%Variation = \frac{(2.56+2.44)}{(22.3+14)} \times 100 = 13.77\%$.

In the same way as the previous study, we look here to compare the predicted results obtained with the couple of friction coefficients (μ=0.12 / μ=0.08). Figures 5a–c report the simulated springback sequences, and highlight the calculated displacement histories. It can be seen from these iso-values a non-uniform distribution of the final displacement and that the limit values determined with a higher friction coefficient (μ=0.12) are larger than the numerically predicted values with a lower one (μ=0.08). As it can be observed from Fig. 5c, a relative difference of displacement obtained with these two considered coefficients of friction varies from −2.77 mm to 2.57 mm, and therefore the relative variation expressed as a percentage is equal to:

$$\%Variation = \frac{(2.57+2.77)}{(22.3+14)} \times 100 = 14.71\%.$$

It can be seen clearly that a percentage of variation almost similar (around 14%) is obtained when a comparison between (μ=0.08 to μ=0.12) and (μ=0.16 to μ=0.12) is done.

In Fig. 6a, b and c the results for the springback of the unloaded structures are presented in order to compare between both coefficients of friction, μ=0.16 to μ=0.08 considered as a
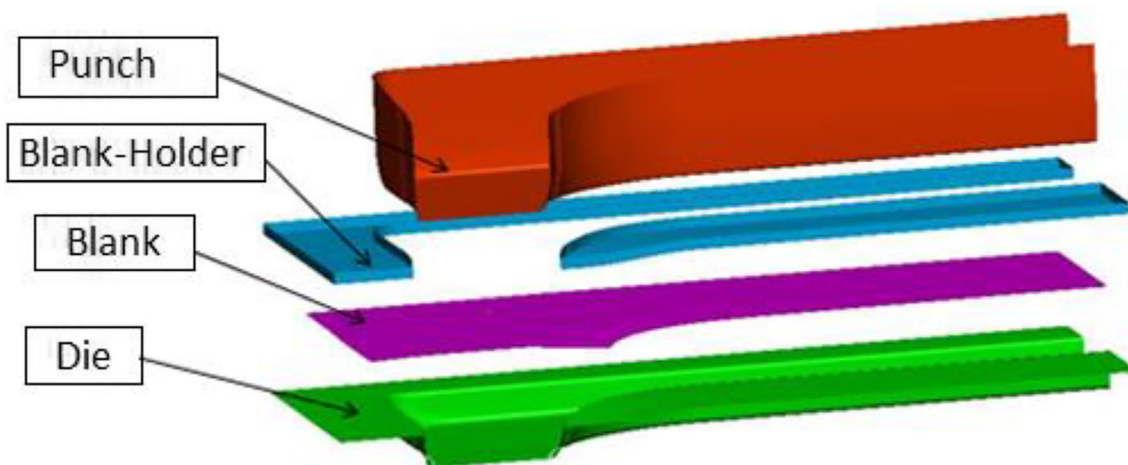

Fig. 3 Three-dimensional exploded view of numerical model used in the deep drawing of the side sill closing
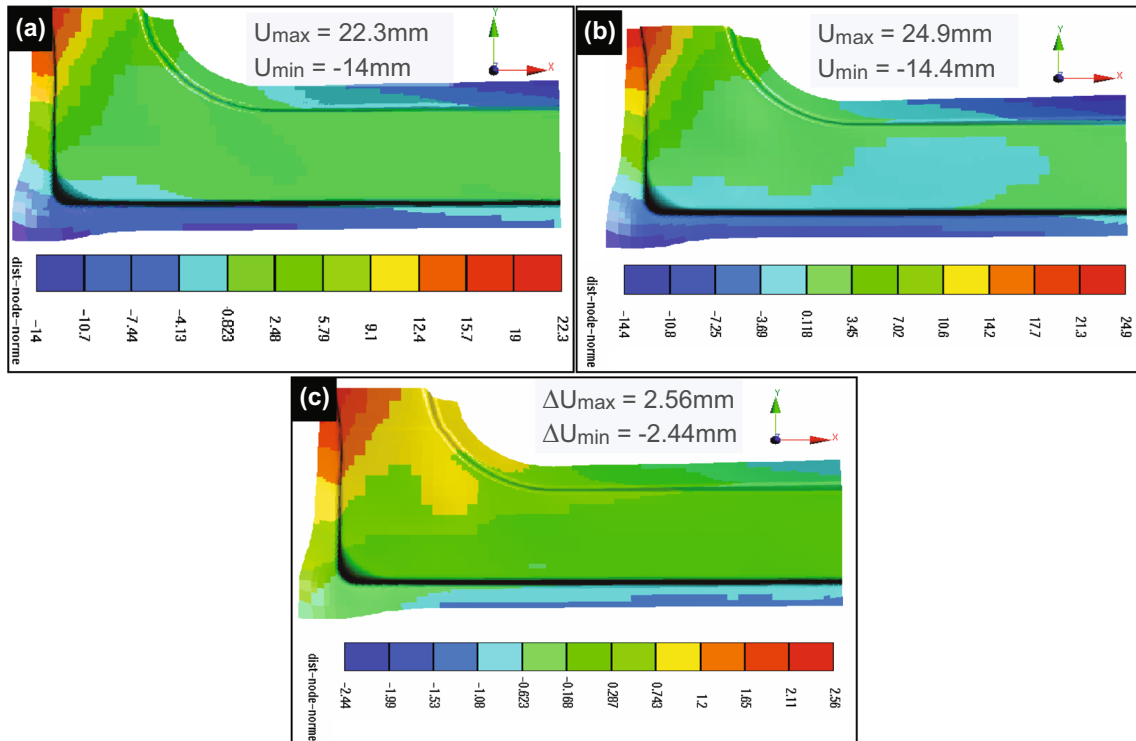
Fig. 4 The displacement isovalues obtained after springback for TRIP800 steel sheet and SHS isotropic hardening behavior law for: **a)** $\mu = 0.12$, **b)** $\mu = 0.16$ and **c)** Relative displacement between two coefficients of friction ($\mu = 0.16/0.12$)
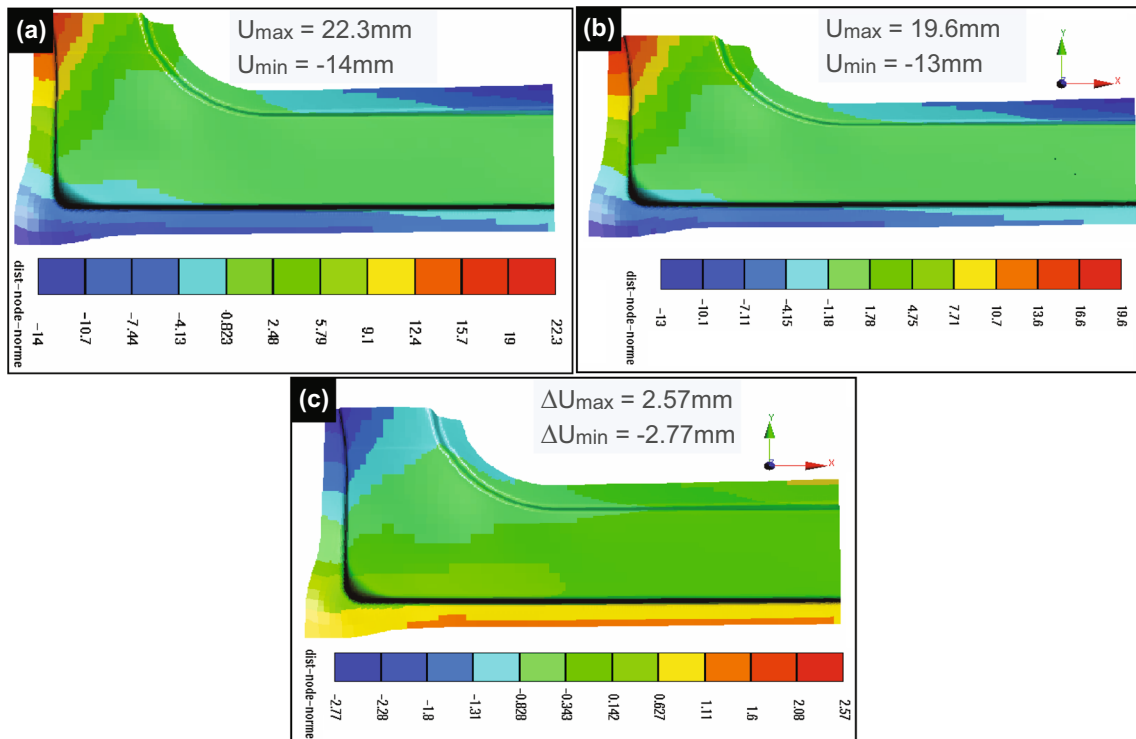

Fig. 5 The 3D iso-values of the final displacement distributions occurring during springback steps, after deep drawing of TRIP800 material and including the SHS isotropic-hardening elasto-plasticity model: **a)** $\mu =$ 0.12, **b)** $\mu = 0.08$ and **c)** Relative geometric difference given in terms of displacement, corresponding to ($\mu = 0.08/0.12$)
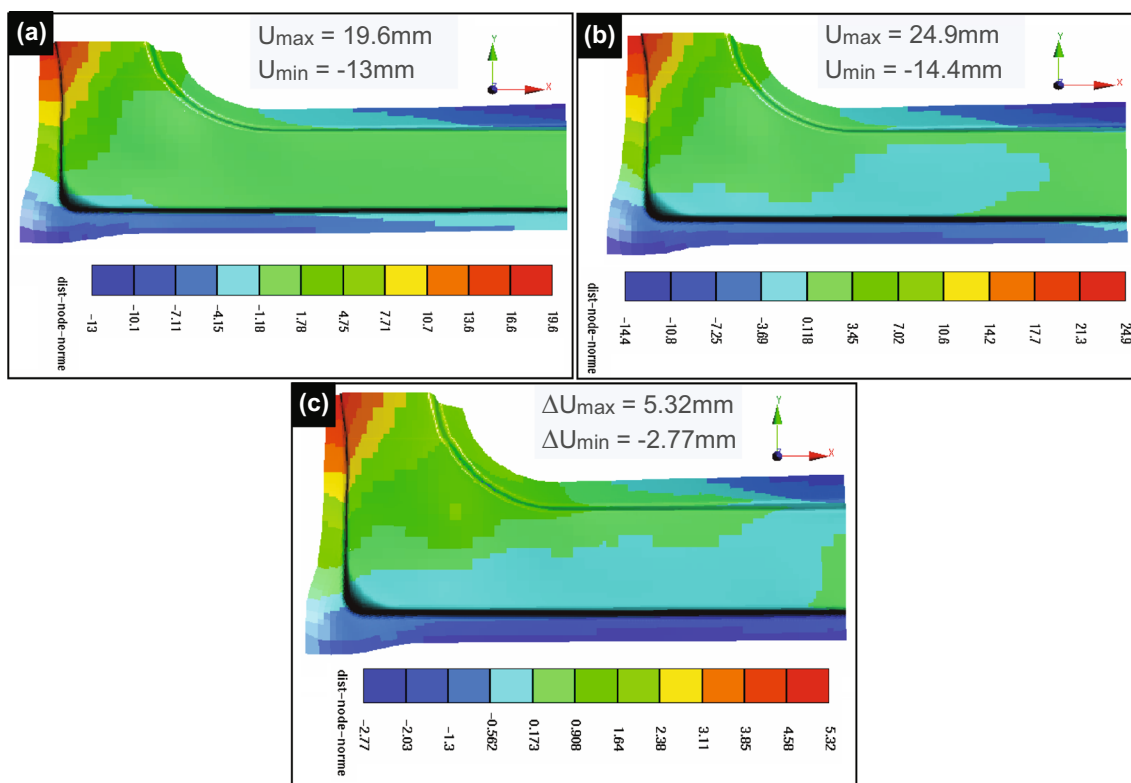
Fig. 6 The results of springback prediction after unloading given in form of displacement distributions on TRIP800 steel sheet and for SHS law describing the isotropic hardening behavior: **a)** $\mu = 0.08$, **b)** $\mu = 0.16$ and

c) Relative difference in displacement computed with these two coefficients of friction 0.08 and 0.16, respectively

reference value. The relative variation of displacement given in percentage is defined by the following expression:

$$\%Variation = \frac{(5.32 + 2.77)}{(19.6 + 13)} \times 100 = 22.28\%.$$

As it can be noted, the percentage of variation increases when we compare between the lower friction coefficient (μ=0.08) and the upper one (μ=0.16). Indeed, it could be predicted that with the increasing of the friction coefficients this variation augments in a remarkable way. This variation is obtained, mainly by the twist phenomenon produced at the bottom and the top of the side sill closing as demonstrated by Fig. 6c. In fact, it can be concluded from the results obtained in Figs. 5 and 6, that the coefficient of friction has a lot of influence, clearly observed, on the springback prediction.

A comparison between the variation of displacements (ΔU=U_{max}-U_{min}) for the three coefficients of friction (μ = 0.08, μ = 0.12, μ = 0.16) is summarized in Table 1. It can be deduced that the variation between maximum and minimum iso-values increases when the friction coefficient increases.

Table 2 presents a summary of results characterizing the percentages of variation reached for different couple of friction coefficients (μ = 0.16/0.12, μ = 0.08/0.12, μ = 0.08/0.16). It can be deduced that the maximum relative error given in

percentage of the displacement variation was obtained for a couple of friction coefficient(μ = 0.08/0.16), corresponding to a value of 22.28%.

The obtained numerical results were compared with the experimental ones. To get some details on the springback of the side sill closing, the stamped part profiles were evaluated in three different sections displayed in Fig. 7. The use of these approaches will lead to a sensitivity analysis of the friction coefficient on the evolution of geometrical profiles. Section 1 and 2 are located on the left and right side of the automotive part, respectively. The third section is located at

Table 1 Comparison of different results characterizing the variation of displacements attained for varied values of friction coefficients

(Material type: TRIP800 advanced high strength steel) and (work–hardening model: SHS law)

Friction coefficients	Variation of displacements (ΔU=U_{max}-U_{min})
(μ=0.08)	32.6 mm
(μ=0.12)	36.3 mm
(μ=0.16)	39.3 mm

Table 2 Percentage of the displacement variation obtained for different couples of friction coefficients

(Material type: TRIP800 advanced high strength steel) and (work–hardening model: SHS law)

Variation of friction coefficients	Relative percentage error
(μ=0.16/0.12)	13.77%
(μ=0.08/0.12)	14.71%
(μ=0.08/0.16)	22.28%

the corner between section one and two. Figure 7 shows the coordinate system used for profile evaluation.

The profile of the part was predicted numerically before and after springback. Figure 8a presents the results of the springback obtained in section 1 by experimental measurements and numerical tests for different coefficients of friction. It can be noted a remarkable opening of the first section after springback. Indeed, the minimum opening is obtained with high value of friction coefficient (μ=0.16). The results corresponding to the friction coefficient of 0.12 is much closer to that found with a coefficient of friction of 0.08. It can also be noted that the measured part profile shows more opening in the region corresponding to the X variation between −190 mm and −150 mm.

In Fig. 8b, the numerical findings and experimental measurements have been recorded at section 2 for various coefficients of friction. It can be clearly noticed, a maximum opening of the second section after springback appearance is localized in the radial direction X, limited between −30 mm and 50 mm. All numerical results obtained by FE simulations for different coefficients of friction are globally very close to the experimental measurements, nevertheless a slight difference of geometrical profiles of the stamped parts could be reported, and situated located in the interval $X \in [−240; −160]$ mm.

The springback and corresponding dimensional deviations reported in section 3 are displayed in Fig. 8c. For the validation of these numerical results relative to a variation of the coefficient of friction, we chose to compare the side sill closing profile formed by deep drawing process in previous experimental works. It was found that all section openings after springback are almost close to each other, and there is a remarkable difference between numerical simulation and experimental data in the right upper corner of the part. The numerical results obtained with a friction coefficient of μ=0.12 is much closer to the profile of the part measured experimentally after springback. It can also be concluded that the friction coefficient has an important impact on these results defined by the springback predicting.

Influence of constitutive laws

In this section, the sensitivity of the constitutive laws using Hill'48 criteria was studied. The forming and springback simulations are performed using PAM-STAMP 2G software. Three types of hardening models (Swift, Hockett-Sherby and SHS laws) were implemented to describe the isotropic work-hardening, and a mixed isotropic kinematic hardening law is also implemented to define the isotropic and kinematic of the work-hardening. In the presented section, the same material TRIP800 is employed and the coefficient of friction is fixed to μ=0.12. Springback analysis was conducted for the

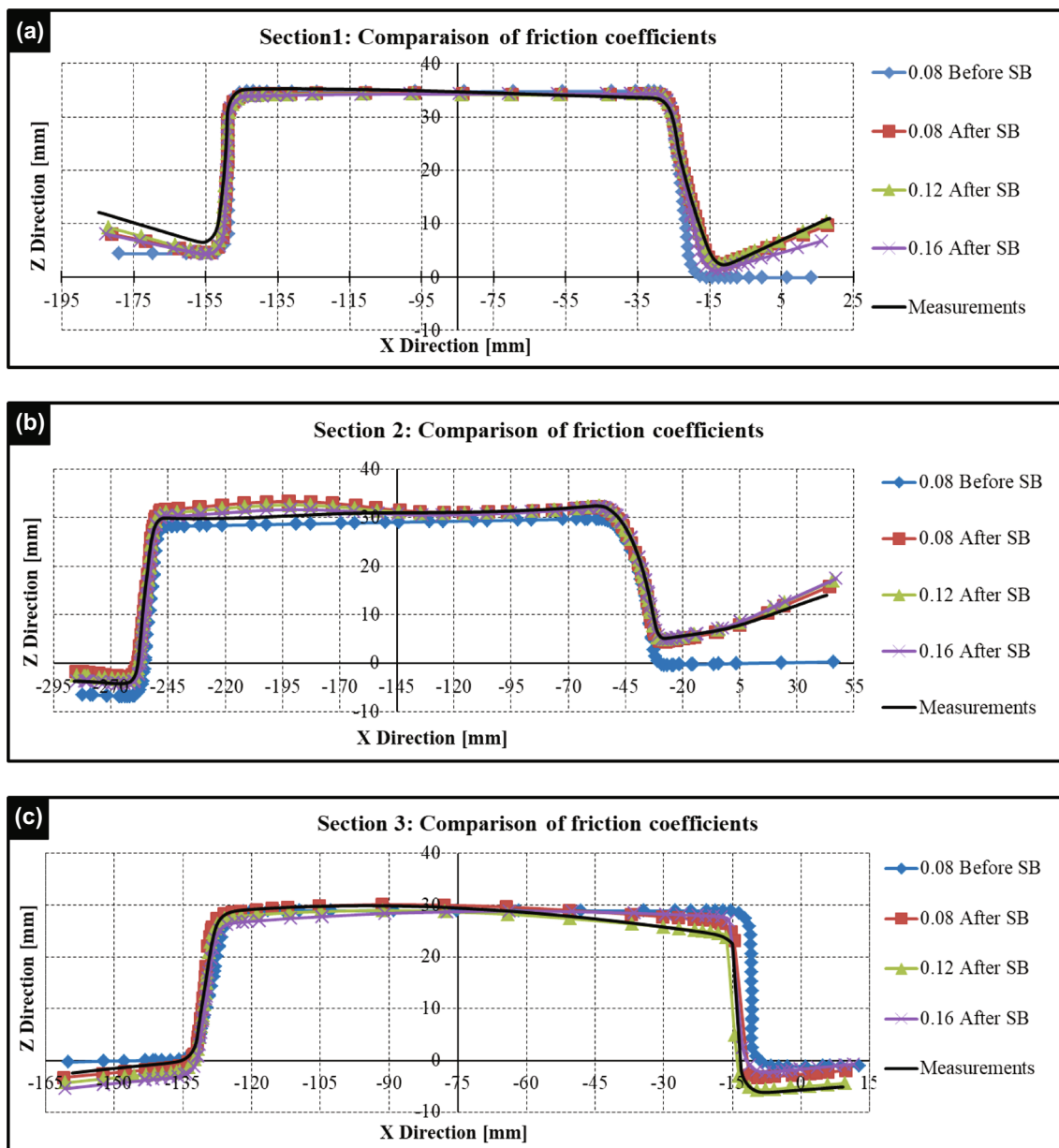**Fig. 7** Section positions in real part used for profiles evaluation
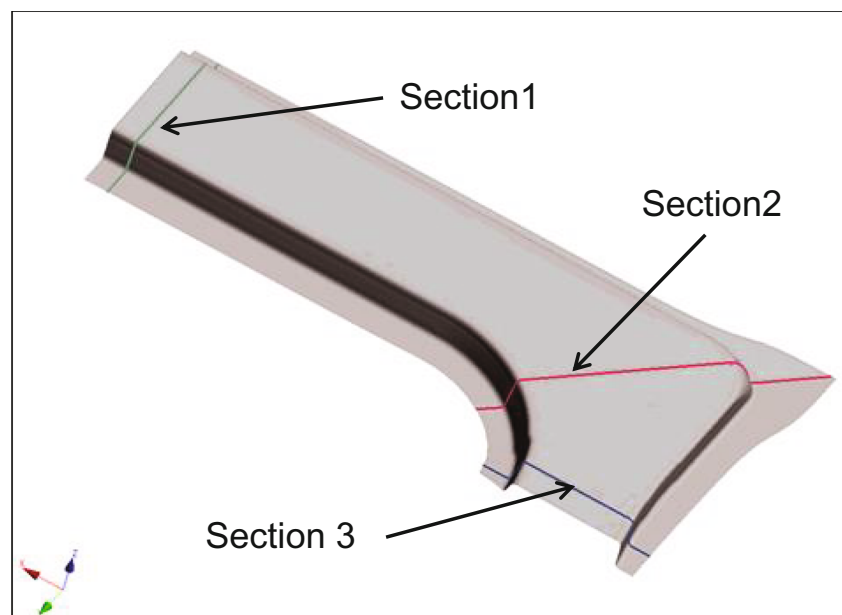
Fig. 8 Comparison of experimental and simulating results corresponding to cross-section profiles evolution obtained before and after springback by mean of deep drawing process under different friction coefficients: measured and predicted profiles in **a)** Section 1, **b)** Section 2 and **c)** Section 3

different constitutive laws; the obtained numerical results were compared with the experimental values in three sections of the formed part. Figure 9a represents the isovalues of the displacement obtained after springback appearance by considering the TRIP800 material and Swift law. The maximum and minimum values of displacement can reach 20.8 mm and −13.5 mm, respectively. Firstly, it can be seen a nonuniform distribution of displacement in the final deformed piece. Secondly, this response in the central region of the bottom of the of the side sill closing remains unchanged, whereas the resulting springback was found to be considerable in the periphery of the part.

The variation of the displacement obtained after springback for the same material and the Hockett-Sherby law is illustrated by contour plots shown in Fig. 9b. As mentioned in this figure, it can be marked that the effect of the constitutive modeling of the real material appears very significant when the extreme values of the relative displacements are observed to be 22.9 mm and −14.1 mm, respectively. These critical responses are predicted in the same forming regions as the results expressed from previous figure.

In order to make a more fair comparison of the models, this geometrical accuracy is also directly reflected to the
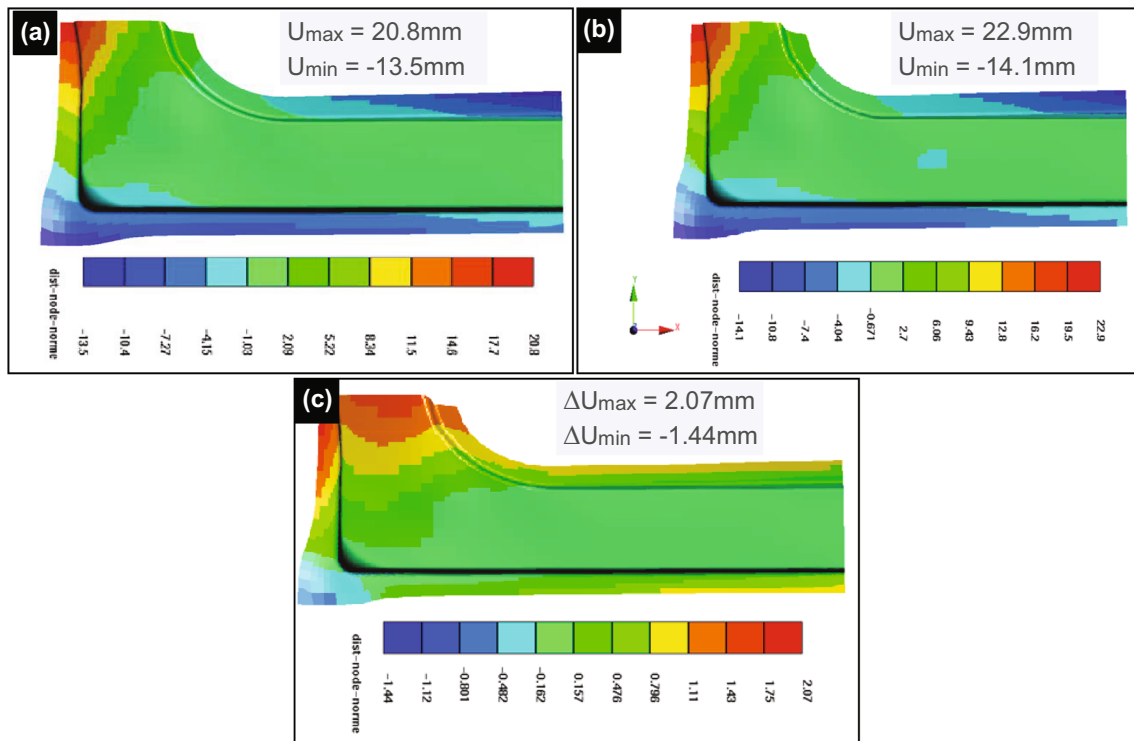
Fig. 9 The three-dimensional displacement distribution in the final deformed pieces resulting from numerical simulation corresponding to the following data (Material: TRIP800; Friction coefficient: $\mu = 0.12$; Yield function: Hill'48 criteria): **a)** Swift isotropic hardening law, **b)** Hockett-Sherby isotropic hardening law and **c)** The differences in simulated displacement distribution using the two considered hardening models

springback results in Fig. 9c where the two considered hardening models (Hockett-Sherby and Swift) deliver the differences in simulated displacement distribution. Small variations of relative displacements are observed when the positive and negative differences are equal to $\Delta U_{max} =$ 2.07, $\Delta U_{min} = -1.44$ mm.

As shown in Fig. 9c, the relative error calculated between Swift and Hockett-Sherby isotropic hardening law compared to the Swift law that's approximately 10.23%. It was expressed in percentage by the following formulation:

$$\%Variation = \frac{(2.07 + 1.44)}{(20.8 + 13.5)} \times 100 = 10.23\%.$$

Consequently, this result could be considered acceptable and satisfactory, since the overall error remains almost small, which prove the ability and fidelity of both hardening behaviors treated in this section for numerical prediction of forming and springback of car body parts.

Figure 10a and b display the results of variation of the displacement obtained at the end of the stamping and after the appearance of springback, that obtained by using the hardening laws of Swift and the two combined laws Swift-Hockett-Sherby (SHS), respectively. The figures show that the absolute values of the upper and lower deviations of the

displacement prediction in the case of the SHS work hardening law were slightly larger than those of the Swift model. Thus, it was found that the displacement varies between −14 mm and 22.3 mm, corresponding to the minimum and maximum springback responses. Figure 10c presents the relative variation of the geometrical error committed between these two types of hardening rules (Swift and SHS behavior laws). An important remark concerns the distribution of the displacement, which is basically observed to be localized on the bottom surface of the side sill closing, resulting in cambring phenomenon, however in the middle part of workpiece this geometrical response results from the sections opening predicted numerically. The deformed shape obtained from a comparison between Swift and SHS hardening models will lead to an estimated percentage of variation about 7.4%. It can be written in the following form:

$$\%Variation = \frac{(1.5 + 1.04)}{(20.8 + 13.5)} \times 100 = 7.4\%$$

Figure 11a, b and c show the influence of the nature of hardening through a comparison of combined isotropic-kinematic hardening law with the corresponding results from the Swift law, considered as a reference model for the
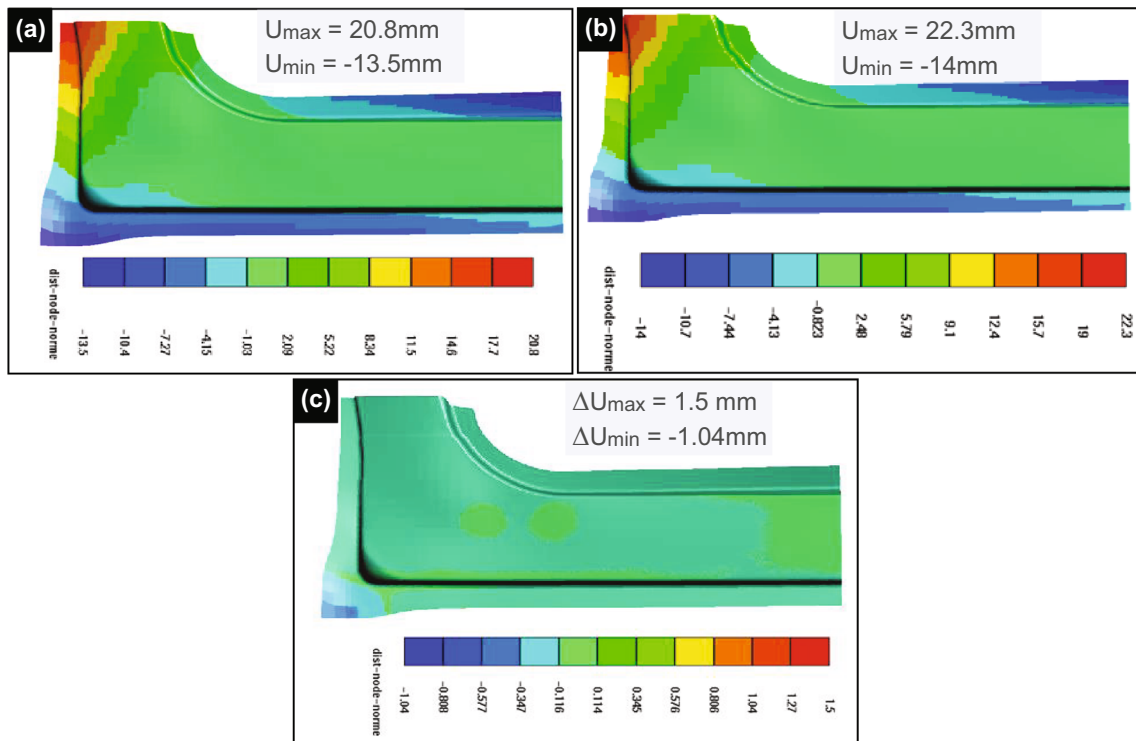
Fig. 10 Contour plot of displacement in the component at the end of the stamping and after springback for material TRIP800, Hill'48 plasticity model and friction coefficient $\mu = 0.12$: **a)** Case of Swift work hardening behavior, **b)** Case of SHS work hardening behavior and **c)** The relative error committed between these two types of hardening rules
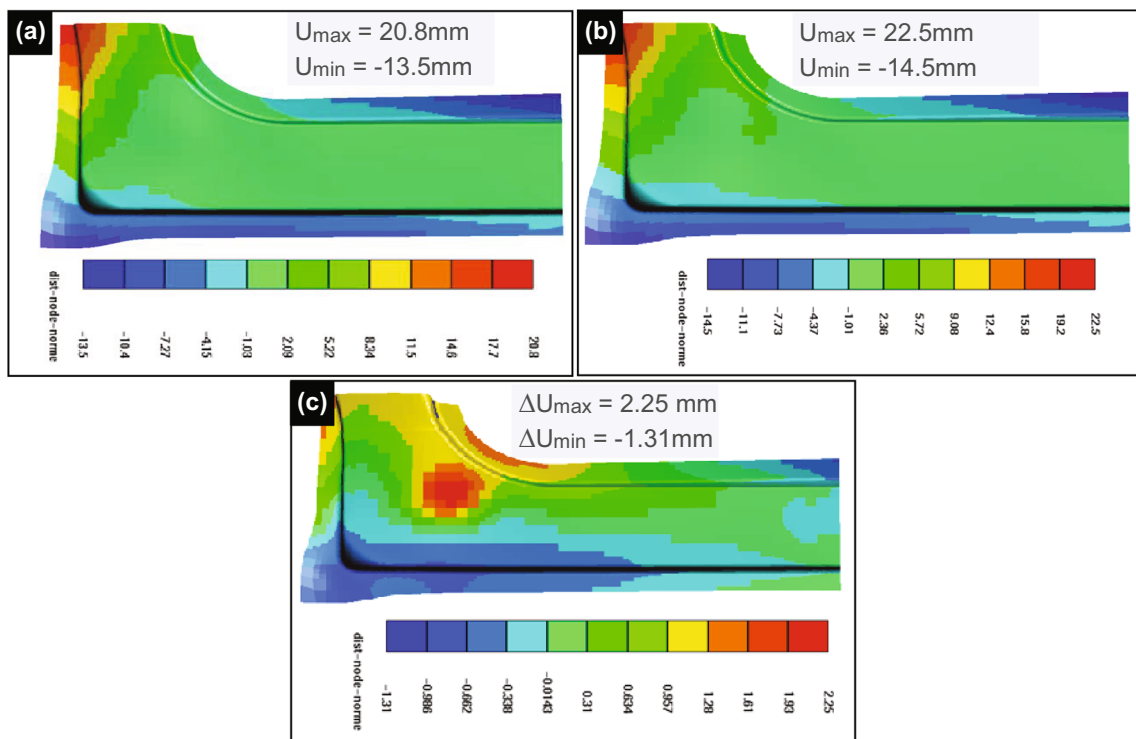

Fig. 11 Comparison between the Swift isotropic hardening law and the mixed isotropic-kinematic hardening model: **a)** Results from Swift law, **b)** Results from combined type of isotropic-kinematic hardening plasticity model and **c)** Displacement differences between isotropic formulation and mixed isotropic-kinematic hardening law

numerical simulation with material TRIP800 material forming by deep drawing process. We remind that the springback geometry studied here is characterized by the relative deviation in displacement between the shape of the deformed product after removal of the sheet metal from the forming tools, compared with its target geometry (the die cavity) generated by computer-aided design. The latter is considered as reference geometry.

Based on the Fig. 11b displaying the contours of displaced shape after unloading, and associated with a mixed nonlinear hardening elastoplastic model it can be indicated that the maximum variation of relative displacement predicted by the numerical model is about 22.5 mm and the minimum displacement is equal to −14.5 mm. This is mainly due to twist phenomenon resulting at the bottom region of side sill closing. For a quantitative evaluation of the influence of hardening behavior type of TRIP800 steel sheet on the geometrical field's distribution, a geometrical shape error is reported in Fig. 11c given in form of contour plots and reproducing the geometrical deviation in terms of resulting displacement. From this contour plots, it can be noted a small dependence of the deformed sheet on the constitutive behavior of sheet material, which can lead to inhomogeneous displacement distributions in the final part. As it can be observed, the predicted displacement continually decreases stepwise through the forming process from its maximum value ($\Delta U_{max} = 2.25$ mm) until reaching its minimum value ($\Delta U_{min} = -1.31$ mm). The comparison of the predicted displacements obtained from the developed models was conducted, and the percentage error is calculated as following:

$$\%Variation = \frac{(2.25 + 1.31)}{(20.8 + 13.5)} \times 100 = 10.38\%$$

Compared to the isotropic hardening results (Swift, Hocket-Sherby and SHS), it is clear that the mixed isotropic-kinematic hardening law has a higher influence on the prediction of the springback.

In this part of work, one undertakes a comparative study between all results provided by the four behavior laws described previously in order to ensure the validity of each one of them for the prediction of relative error values of springback. Table 3 recapitulates the percentage of the relative variation of the resulting displacement obtained with different constitutive models. Consequently, it can be concluded that both the isotropic hardening laws (Swift, Hockett-Sherby and SHS) and the combination of isotropic and kinematic hardening law (Mixed law) showed a minor influence on the springback prediction. Indeed, the maximum variation does not exceed in any case 10%, judged to be satisfactory. The obtained results also prove that the constitutive laws have a lower influence when they will be compared to the friction coefficients (see Table 2).

Table 3 Calculated relative error, expressed in terms of percentage of the displacement according to the isotropic constitutive model of Swift's strain hardening.

The comparison of the part profile from FEM simulation before and after springback with the experimental results after stamping and springback is displayed in Fig. 12a, b and c, corresponding respectively, to the section 1, section 2 and section 3 (see Fig.7 for more details about the section positions).

After final unloading, an opening of geometrical profiles could be reported in sections 1 and 2, but the inverse phenomenon has occurred in section 3 after springback showing remarkable closures of profiles. A good correlation between measurements and simulations were therefore observed in sections 1 and 3. Nevertheless, throughout the radial direction of section 2 (see Fig. 12b) a slight deviation between the numerical results and the experimental measurements can be noticed, especially for a radial distance defined by X > 0 mm.

Comparison of different yield functions

After having studied the effect of the material-hardening mode on the springback prediction by using the Hill'48 yield function, the influence of the yield criteria on the prediction of the springback will now be investigated. For that purpose, three yield loci including the Hill 48, Hill 90 and Barlat 91 functions were implemented in Pam-Stamp 2G software and were compared. The same material (TRIP800) and the isotropic SHS law have been considered for numerical simulation for the rest of this research works. Figure 13a, b and c display the results of distribution of the displacement after springback. The computed result with Hill 48 yield function leads to minimum and maximum values of displacement, respectively, equal to $U_{max} = 22.3$ mm and $U_{min} = -14$ mm. Figure 13b shows the springback variation related to the yield loci based on the Hill 90 in order to examine the geometrical state of the stamped part at the end of this operation and after springback appearance. The same figure verifies the

Table 3 Calculated relative error, expressed in terms of percentage of the displacement according to the isotropic constitutive model of Swift's strain hardening

(Material type: TRIP800 High Strength Steel) and (coefficient of friction: μ=0.12)

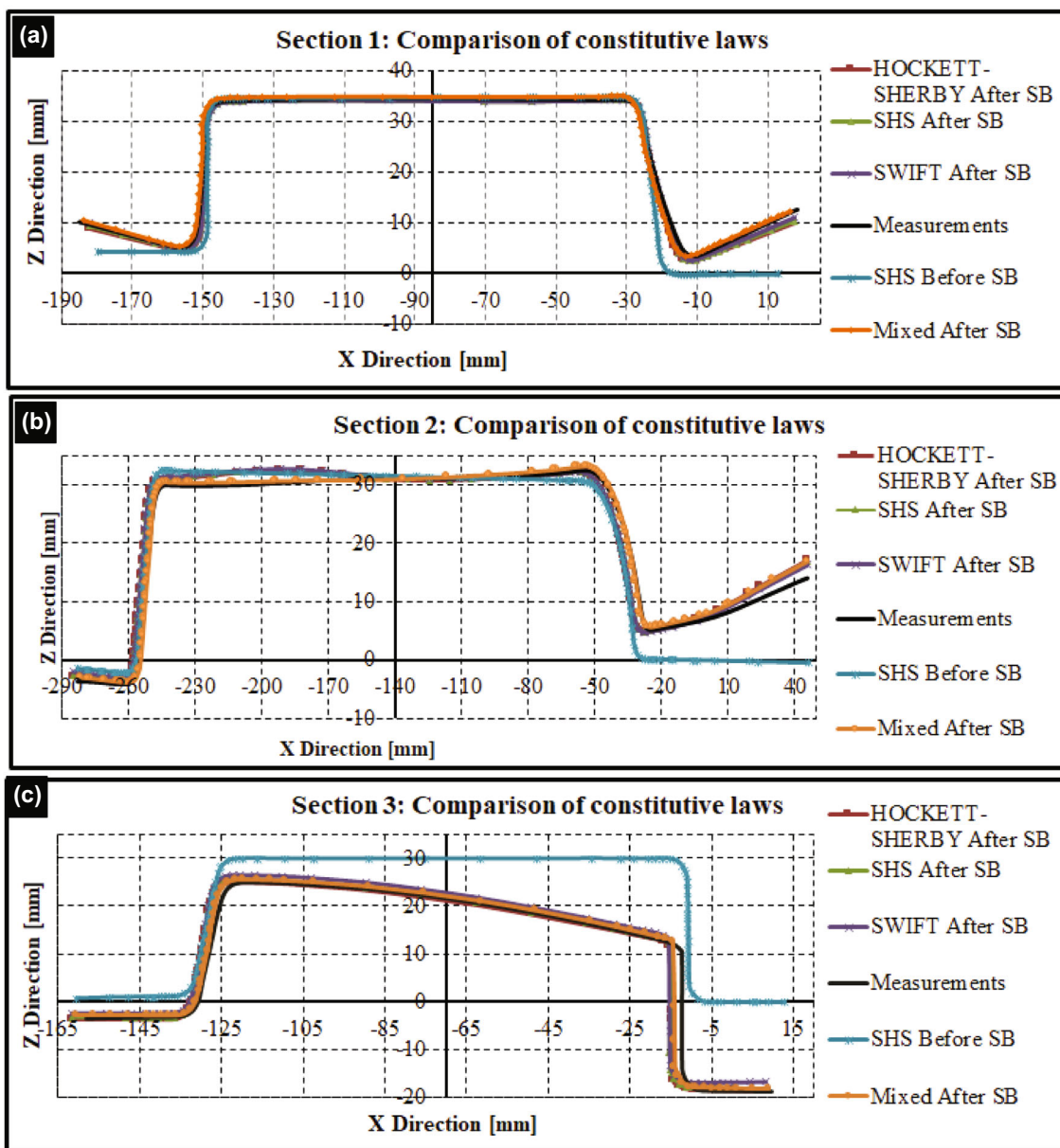| Various tested hardening laws	Comparison of relative displacement
(Hockett-Sherby/Swift)	10.23%
(SHS/Swift)	7.40%
(Mixed/Swift)	10.38%

Fig. 12 Comparison of the part profile from FEM simulation before and after springback with the measured results after stamping and removal of tools in: **a)** Section 1, **b)** Section 2 and **c)** Section 3

expected higher values of the springback errors prediction in the deep drawing, which are located in the deformed lower region near the contour of the part. It indicates the change in the distribution of the relative displacement in the fully unloaded state, where the red and dark blue colors represent higher and lower values, respectively. By examining the 3D iso-values of the geometric error of the sheet springback obtained by FEM calculation and given by Fig. 13a and b, the predicted results using Hill'48 yield criterion seem to be clearly larger than those determined with of Hill 90.

From simulation result, the relative gap resulting from the significant difference in displacement between the two

different cases of Hill 48 and Hill 90 was plotted in Fig. 13c. As it can be seen from this figure, two phenomena are of big interest: the twist at the top of the side sill closing and side wall curl. The difference in springback between the considered material models defining the relative variation in terms of residual displacement is measured as a percentage, and can be expressed in the following form:

$$\%Variation = \frac{(5.04 + 5.24)}{(22.3 + 14)} \times 100 = 28.32\%$$

At this point, it should also be noticed that this value of the estimated relative error is more pronounced than the overall error results calculated from the comparison of different
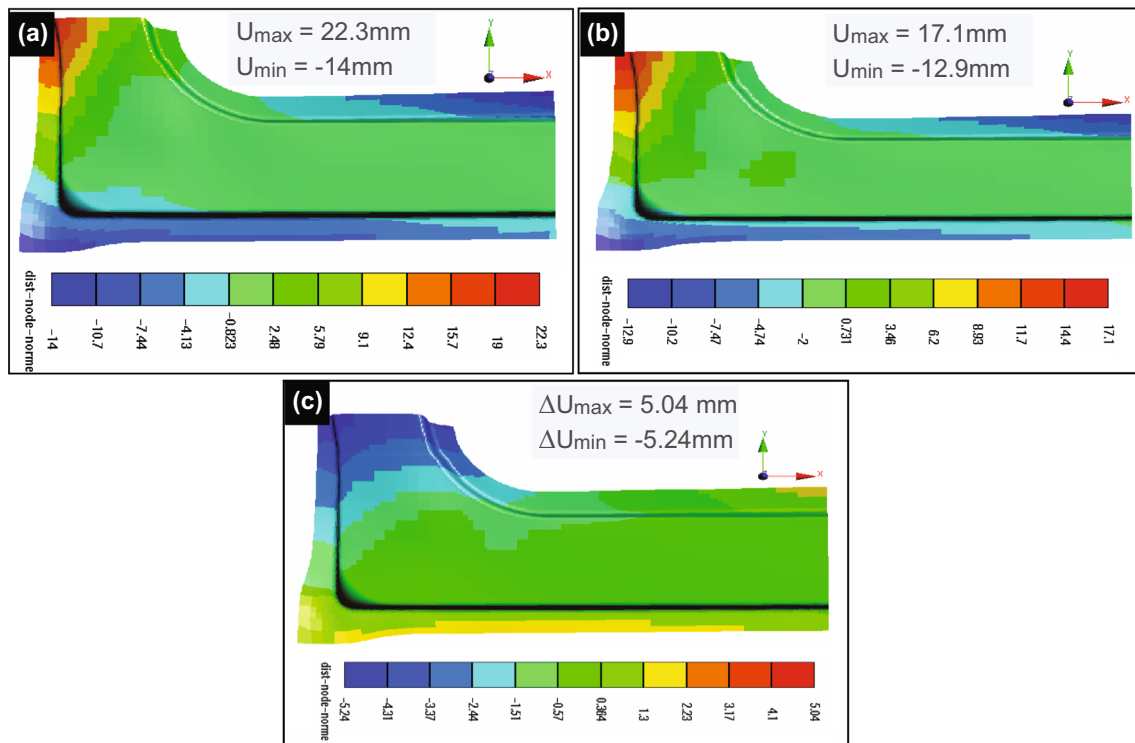
Fig. 13 Displacement repartition obtained after springback when the TRIP800 steel material and a value of friction coefficient $\mu = 0.12$ are used in combination with the isotropic SHS hardening model: The computed result with **a)** Hill'48, **b)** Hill'90 yield functions and **c)** Difference in springback between material models Hill'48 and Hill'90

coefficients of friction and the influence of various constitutive laws mentioned previously (see Tables 2 and 3).

The predicted findings presented in Fig. 14 investigate the final geometrical shape of the automotive part resulting in appearance of springback. The effectiveness of the developed approach is evaluated through a comparison of numerical results obtained with Barlat91 yield function to those found by using Hill 48 material model. The contour plots distribution of the deformed shape predicted by the Barlat'91 yield criterion is shown in Fig. 14b. It allows displaying the evolution of the relative displacement caused by springback after forming and retracting the tools. For this simulation, the springback was calculated by considering the normal direction to the inner surface. The displacement variation between the inner and outer surface of the sheet for the whole part presents a major deviation between maximum and minimum values, equal to 22.1 mm and −13.5 mm, respectively. From the results indicated in Fig. 14a and b, it could be observed that the upper and lower deviations characterizing the interval of springback variation are globally close and follow almost the same order of magnitude for both Hill 48 and Barlat'91 material models.

Figure 14c depicts the relative difference in displacement calculated from the two previous yield criteria. From a numerical point of view, the springback deviation based on residual stresses cannot exceed the maximum value of 1.41 mm, however its minimum is limited to −1.01 mm.

From the 3D plot of contours shown in Fig. 14c, it was concluded that the main difference between results determined from the two plasticity models could be due to a cambering phenomenon. In fact, the maximum and minimum variations are localized on the top and on the bottom of the side sill closing, respectively. The relative percent difference compared to the Hill 48 yield function considered as reference model was computed according to the following expression:

$$\%Variation = \frac{(1.41 + 1.01)}{(22.3 + 14)} \times 100 = 6.66\%$$

In order to make a comparative study between all results determined by different yield functions, we chose to recapitulate in the same table all relative displacement variations expressed as a percentage of Hill'48 yield criteria. A comparison of the calculated results of relative springback errors for both material models Hill 90 and Barlat 91 has been summarized in Table 4. In fact, according to the numerical results presented in this table, it is clearly observable the decrease of the relative percent difference for the displacement values when a comparison of Barlat91 with Hill90 yield criteria is done. It was found that the difference between (Barlat 91 and Hill 48) yield locus is smaller than that calculated in the case of the couple (Hill 90 and hill 48) yield functions. Consequently, the smallest and highest values of the relative
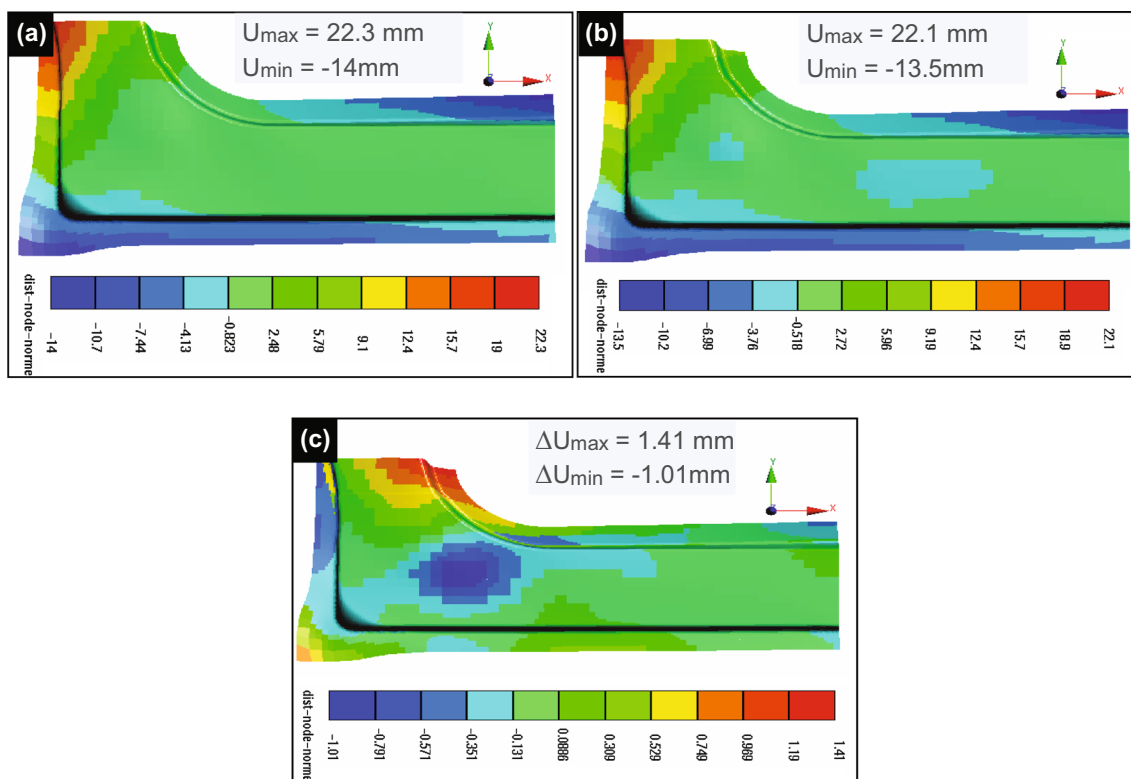
Fig. 14 Contour plots of the deformed shape displaying the displacement variation in workpiece after forming for the same numerical conditions applied in the previous test: a) Case of Hill'48 yield criterion, b) Case of yield stress function proposed by Barlat'91 and c) Difference in simulation results using Hill'48 yield loci compared to Barlat'91 plasticity model

springback variation are consecutively 6.66% and 28.32%, reached for Barlat 91 and Hill90, respectively. These mentioned yield functions were compared to the Hill 48 yield criterion employed as a reference material model. It may be reasonably assumed that this remarkable value of the maximum variation controlled from numerical simulations is mainly due to the twist phenomenon produced at the bottom of the side sill closing (see Fig. 13b). In conclusion, it can be seen from this part of analysis a considerable influence of the yield locus on the prediction of the springback and that the material model strongly effects the final shape of formed sheets.

Figure 15 represents a correlation between the experimental cross section geometries measured along the X-axis and the numerical profiles predicted from FE simulations. They were evaluated in 3 different sections of the stamped part of the side sill closing workpiece. A good agreement between experimental and numerical results can be observed after the appearance of springback in sections one and two. From these results, the obtained profiles after stamping seem to be almost identical for every material model. As shown in Fig. 15a and b, the two models Hill48 and Barlat91 yield functions may also lead to results very close. As illustrated in Fig. 15b, it can be clearly seen some slight deviations explained by a distortion of the manufactured parts. Moreover, there is an

observable opening localized especially beyond the right corners of the formed parts. For comparison purposes of all previously mentioned yield criteria, Fig. 15c illustrates the finite element results for section 3 which are subsequently superimposed with the experimental measurement. While referring to this considered figure, it is possible to deduce two observations:

The first is related to the geometrical aspects of the stamped part where all cross-sectional profiles resulting from both FEM simulations and experimental tests after springback are visibly distorted showing a notable deviation. Additionally, it was found another phenomenon which characterizes the cambering and bending effect denoted by an excessive orientations and deformations of the specimens during the forming step. These findings, have been proven for various material models implemented into Explicit finite element code Pam-Stamp, describing various yield criteria.

The second observation concerns the comparison in terms of geometrical accuracy of springback between the simulation results of the predicted cross-sectional profiles to the experiment. From a global point of view, it worth noting in Fig. 15c that the different geometrical profiles plotted along the X-axis evolve similarly, while following almost identical variations with the same accuracy, with the exception of Hill 90 yield
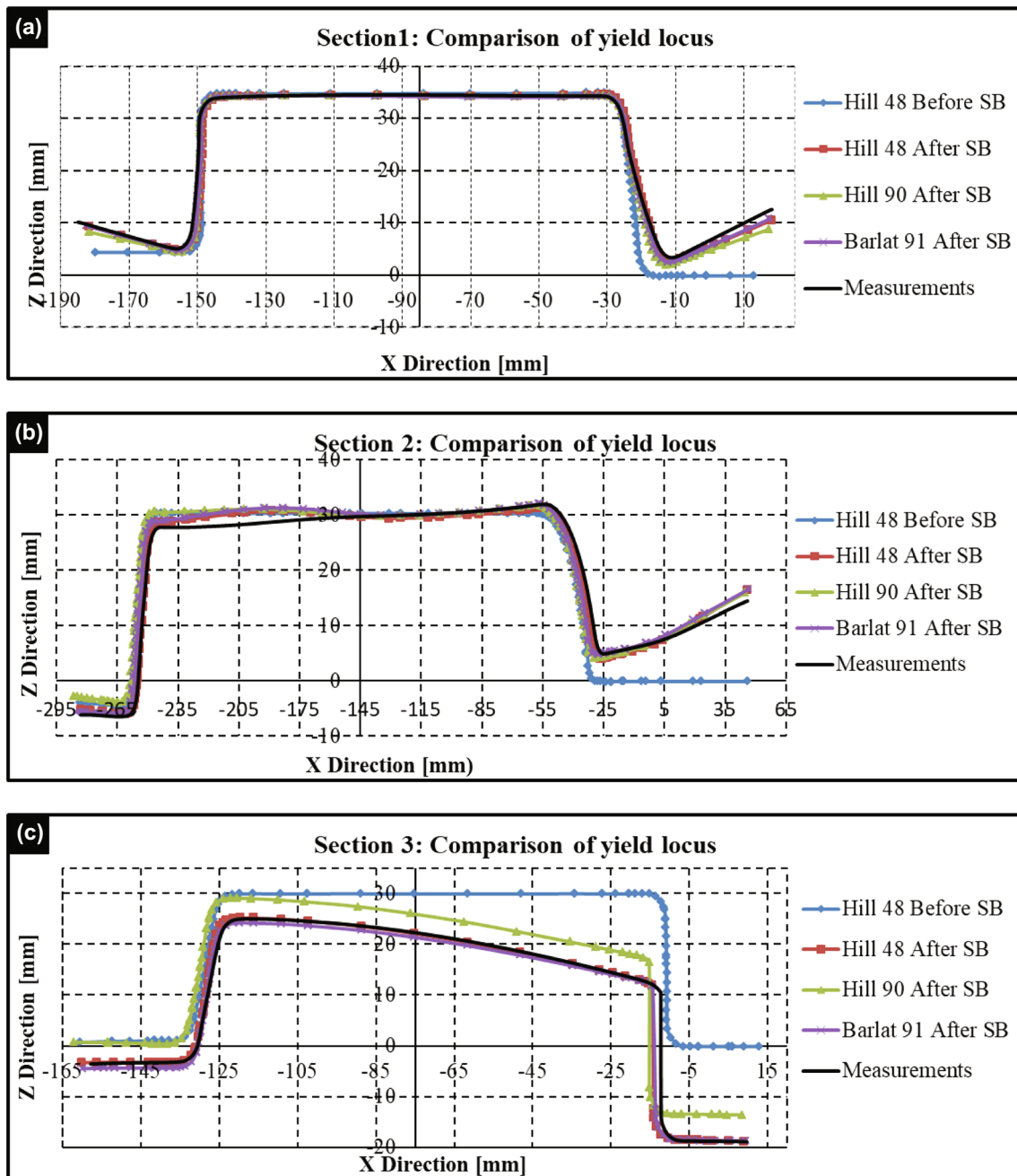
Fig. 15 Evolution of the experimental cross section geometries measured along the X-axis and the predicted profiles resulting from the numerical simulations in 3 different regions of the structure of side sill closing. The comparison of the yield functions in: **a)** Section 1, **b)** Section 2 and **c)** Section 3

function which gives results with more deviation compared to the measurements and to other material models.

Finally, in conclusion of this section, and based on the results presented by Fig. 15a, b and c and on the Table 4 recapitulating the relative displacement variation obtained for different couples of yield loci and expressed as a percentage of Hill'48 yield criteria, it can be confirmed that the material models have a considerable impact and a significant role on the predicted springback errors.

Conclusion

In this study several material laws are evaluated in order to determine their influence on the prediction of the springback. The constitutive models are used to allow the different aspects of materials mechanical behavior to be better described: isotropic work-hardening (Swift, Hockett-Sherby, SHS), isotropic-kinematic hardening, yield loci (Hill 48, Hill 90 and Barlat 91). The effects produced by these

Table 4 Relative displacement variation obtained for different couples of yield loci and expressed as a percentage of Hill'48 yield criteria

(Material type: TRIP800 Advanced High Strength Steel, AHSS), (Friction coefficient: μ=0.12) and (Type of strain hardening formulation: isotropic SHS law)

Material models (Type of yield loci)	Comparison of relative displacement
(Hill90/Hill48)	28.32%
(Barlat91/Hil48)	6.66%

abovementioned material models on the springback of High Strength Steel TRIP800 was investigated and compared to the influence of friction behavior. It is recognized that the friction is one of the process parameters that has a lot of influence on the springback predictions. The obtained results confirm this tendency for the industrial example (side sill closing) and for the steel TRIP800 used in automotive industry. Based on the obtained measurements and numerical results, the following conclusions can be made:

1. This study allowed us to classify these parameters by order of importance

*   The first parameter that has a big impact on the prediction of springback is the yield loci (Hill 48, Hill 90, Barlat 91). The side sill closing example showed a maximum sensitivity around 28%.
*   The second parameter represents the friction; the obtained results showed a sensitivity about 22%;
*   In the third classification, we will find the least significant factor, representative of the work-hardening laws (Swift, Hockett-Sherby, SHS, mixed). Accordingly, the smallest value of sensitivity was around 10%.

2. The combined isotropic-kinematic hardening law seems to have the same sensitivity as the isotropic work-hardening (Swift, Hockett-Sherby, SHS)
3. In this case of deep drawing process, the numerical model with isotropic-Kinematic work-hardening and yield loci Hill 48 fits well with experimental results.
4. The maximum deviation between measurements and numerical results was obtained for the isotropic work-hardening SHS and yield loci Hill 90.

Compliance with ethical standards

Conflict of interest The authors declare that they have no conflict of interest.

Code availability Commercial code Pamstamp 2G.

References

1. Grueebler R, Hora P (2009) Temperature dependent friction modeling for sheet metal forming. Int J Mater Form 2(S1):251–254. https://doi.org/10.1007/s12289-009-0548-z
2. Santos AD, Teixeira P (2008) Study on experimental benchmarks and simulation results in sheet metal forming. J Mater Process Technol 199(1-3):327–336. https://doi.org/10.1016/j.jmatprotec.2007.08.039
3. Keum YT, Wagoner RH, Lee JK (2004) Friction model for FEM simulation of sheet metal forming operations. AIP Conf Proc 712:989–994. https://doi.org/10.1063/1.1766656
4. Kim C, Lee JU, Barlat F, Lee MG (2014) Frictional behaviors of a mild steel and a TRIP780 steel under a wide range of contact stress and sliding speed. J Tribol 136(2):021606. https://doi.org/10.1115/1.4026346
5. Julsri W, Suranuntchai S, Uthaisangsuk V (2018) Study of springback effect of AHS steels using a microstructure based modelling.Int J Mech Sci 135:499–516. https://doi.org/10.1016/j.ijmecsci.2017.11.043
6. Lin J, Hou Y, Min J, Tang H, Carsley JE, Stoughton TB (2020) Effect of constitutive model on springback prediction of MP980 and AA6022-T4. Int J Mater Form 13(1):1–13. https://doi.org/10.1007/s12289-018-01468-x
7. Ben-Elechi S, Naceur H, Knopf-Lenoir C, Batoz JL (2012) Approche inverse améliorée pour la minimisation du retour élastique de pièces embouties. European J Comput Mecha 17(3):349–372. https://doi.org/10.3166/remn.17.349-372
8. Quadfasel A, Lohmar J, Hir G (2017) Investigation of springback of high manganese TWIP-steels using three-point-bending. International Conference on the Technology of Plasticity, ICTP 2017, 17–22 September 2017, Cambridge. Procedia Engineering 207(2017):1582–1587. https://doi.org/10.1016/j.proeng.2017.10.1052
9. Lee JY, Barlat F, Lee MG (2015) Constitutive and friction modeling for accurate springback analysis of advanced high strength steel sheets. Int J Plasticity 71:113–135. https://doi.org/10.1016/j.ijplas.2015.04.005
10. Zhang DJ, Cui ZS, Ruan XY, Li YQ (2007) An analytical model for predicting springback and side wall curl of sheet after U-bending. Comput Mater Sci 38(4):707–715. https://doi.org/10.1016/j.commatsci.2006.05.001
11. Laurent H, Grèze R, Manach PY, Thuillier S (2009) Influence of constitutive model in springback prediction using the split-ring test. Int J Mech Sci 51(3):233–245. https://doi.org/10.1016/j.ijmecsci.2008.12.010
12. Oliveira MC, Alves JL, Chaparro BM, Menezes LF (2007) Study on the influence of work-hardening modeling in springback prediction. Int J Plasticity 23(3):516–543. https://doi.org/10.1016/j.ijplas.2006.07.003
13. Broggiato GB, Campana F, Cortese L (2008) The Chaboche nonlinear kinematic hardening model: calibration methodology and

validation. Meccanica 43(2):115–124. https://doi.org/10.1007/s11012-008-9115-9

14. Sumikawa S, Ishiwatari A, Hiramoto J, Urabe T (2016) Improvement of springback prediction accuracy using material modelconsidering elastoplastic anisotropy and Bauschinger effect. J Mater Process Technol 230:1–7. https://doi.org/10.1016/j.jmatprotec.2015.11.004

15. Komgrit L, Hamasaki H, Hino R, Yoshida F (2016) Elimination of springback of high-strength steel sheet by using additional bending with counter punch. J Mater Process Technol 229:199–206. https://doi.org/10.1016/j.jmatprotec.2015.08.029

16. Lemaitre J, Chaboche JL (1985) Mechanical of solid materials. Cambridge University Press, Cambridge

17. Dasappa P, Inal K, Mishra R (2012) The effects of anisotropic yield functions and their material parameters on prediction of forming limit diagrams. Int J Solids Struct 49(25):3528–3550. https://doi.org/10.1016/j.ijsolstr.2012.04.021

18. Pam-Stamp (2015.1) user's guide

19. Barlat F, Lege DJ, Brem JC (1991) A six-component yield function for anisotropic materials. Int J Plast 7(7):693–712. https://doi.org/10.1016/0749-6419(91)90052-Z

20. Hill R (1950) The mathematical theory of plasticity. Oxford University Press, London